Pump-probe spectroscopy of cold ^{87}Rb atoms in various polarization configurations

Ying-Cheng Chen, Yun-Wen Chen, Jung-Jung Su, Jeng-Yu Huang, and Ite A. Yu
Department of Physics, National Tsing Hua University, Hsinchu, Taiwan 300, Republic of China
(Received 5 May 2000; revised manuscript received 11 September 2000; published 14 March 2001)

We investigate systematically pump-probe spectroscopy of cold ^{87}Rb atoms produced by a magneto-optical trap. The pump-probe spectra are measured without the presence of the trapping beams or any optical molasses. Various polarization configurations of the probe and pump fields result in very different spectra of probe absorption. The observed spectra exhibit a dispersive profile, a dispersionlike profile, a Lorentzian profile, or a dispersive profile plus a Lorentzian profile. The widths of all the spectral profiles are narrower than the natural linewidth of the excited state. Our work clarifies the mechanisms behind these different spectral profiles and provides essential information for the pump-probe spectroscopy of cold atoms.

DOI: 10.1103/PhysRevA.63.043808 PACS number(s): 42.65.−k, 42.50.Gy, 32.80.Pj

I. INTRODUCTION

Cold atoms produced by a magneto-optical trap (MOT) [1] provide great opportunities for the studies of quantum phenomena at long de Broglie wavelengths and for the scientific applications that require atoms with slow velocity or low kinetic energy. An atom temperature on the order of 100 μK can be easily achieved with a MOT setup. The Doppler and transit-time effects are greatly reduced at such temperature. One can also obtain rather dense sample of cold atoms and still enjoy negligible perturbations from collisions. Cold atoms are ideal for spectroscopy studies.

Pump-probe spectroscopy is a powerful tool to study atom-photon interaction. When a pump field is applied, the information about the interaction processes and the atomic medium can be extracted from the probe spectra. For example, pump-probe spectroscopy has helped researchers to explore the cooling mechanism and dynamics of a MOT [2–6]; it has also provided more accurate information on the hyperfine structures of many atomic species [7–12].

The pump-probe spectra of cold atoms with widths narrower than the natural linewidth of the excited state are first reported in Refs. [2,3]. In the experiments, the cold atoms are produced with a MOT and the subnature-linewidth spectra exhibit dispersionlike profiles. Reference [2] proposes that the observed spectra are due to the stimulated Raman transition between the Zeeman sublevels in the ground state. This remarkable theory can well explain the experimental observations of Refs. [2,3]. We briefly describe the theory and the work of Ref. [2] below. Two counter-propagating laser beams with opposite circular polarizations and same intensity form the pump field. This results in linearly polarized pump field with the polarization direction rotating in space. Consider the frame whose z axis is in the polarization direction of the pump field. The light shifts of ground-state Zeeman levels induced by the red-detuned pump field are similar to those shown in Fig. 5(c) (that will appear in Sec. IV B). According to the experimental condition, Ref. [2] states that the population distribution among the ground-state Zeeman levels is determined by the trapping field of the MOT and looks like the distribution in Fig. 5(c). The probe field drives $\Delta m = \pm 1$ transitions. For the case in the left drawing of Fig. 5(c), the stimulated Raman transition results in amplification of the probe field; for the case in the right drawing of Fig. 5(c), that results in absorption of the probe field. Therefore, the pump-probe spectrum shows a dispersionlike profile that resulted from the two Lorentzian profiles of the amplification and the absorption. The peak-to-peak width of the dispersionlike profile is determined by the light shifts. From the above description, it is understood that such pump-probe spectra can be used to explore population distribution among Zeeman sublevels of the atoms in a MOT or optical molasses.

With the theory of the stimulated Raman transition in mind, we have found some results in Ref. [13] unclear. The article presents dressed-atom spectroscopy of cold Cs atoms. Some pump-probe spectra in the article also exhibit subnatural-linewidth and dispersionlike profiles. The atomic system (the $|6S_{1/2},F=4\rangle$ and $|6P_{3/2},F'=5\rangle$ states) of these spectra is the same as that of the spectra in Ref. [2]. On the other hand, the spectra of Ref. [13] are measured in a simpler situation that one pump and one probe beams are used and the trapping beams are not present. The authors of the article state that dispersionlike profiles appear only when the pump field is circularly polarized. They also propose ''The subnatural width can be explainable if it is due to a Λ-type stimulated Raman process with a small splitting in the ground state $F=4$ level.'' We search the literature in order to clarify their spectra and their explanation. No satisfactory answer was obtained. This has prompted the motivation for our paper.

We have systematically investigated pump-probe spectroscopy of cold ^{87}Rb atoms in various polarization configurations. The observed spectra can exhibit a dispersive profile, a dispersionlike profile, a Lorentzian profile, or a dispersive and a Lorentzian profiles. Our work clarifies the mechanisms behind these different spectral profiles and provides essential information for the pump-probe spectroscopy of cold atoms. Some features of our paper are summarized in the following. (i) Pump-probe spectra are measured without the presence of the trapping beam and any optical molasses. Only one pump beam and one probe beam are used and their polarizations do not vary with space nor with time in each measurement. This simple situation helps to identify the physical mechanisms behind experimental observations. (ii) The pump and probe beams propagate in the orthogonal directions in most mea-

 ©2001 The American Physical Society

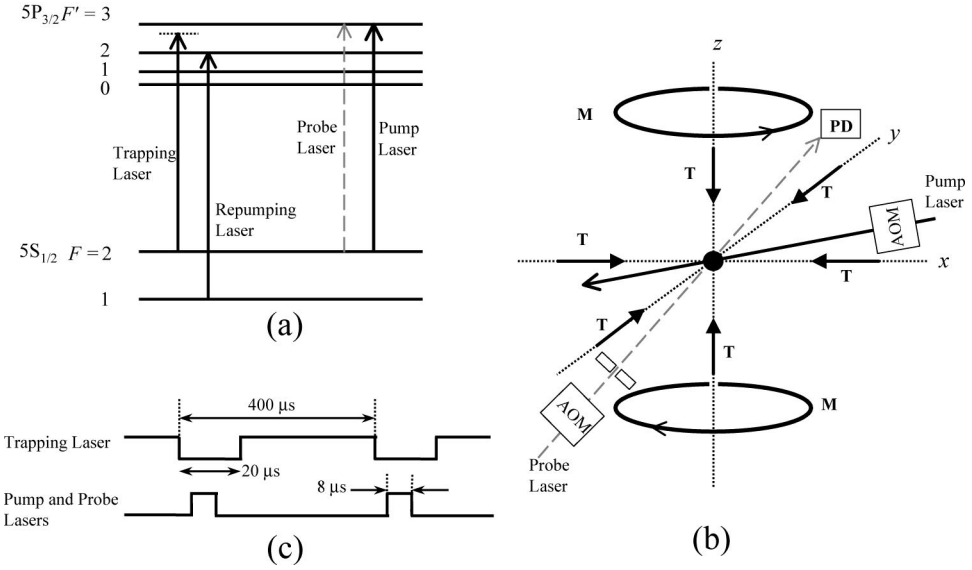

FIG. 1. (a) Energy levels of ^{87}Rb and the excitations of the laser fields. (b) Scheme of the experiment. T denotes the trapping beams and M denotes the anti-Helmholtz coils. The repumping beam is not shown in the figure. The symmetry axis of the anti-Helmholtz coils is in the *z* direction. The pump and probe beams propagate in the *xy* plane. PD is the photodetector for measuring the probe absorption. (c) The timing sequence of the experiment.

surements. Flexibility of the experimental arrangements and degree of freedom of the studies are improved. The orthogonal propagation also prevents the spectra from being influenced by the two-wave mixing between the pump and probe fields [14–17]. (iii) The pump and probe beams interact with atoms in the mode of periodic pulses and the probe frequency is slowly swept. The pulse length is short enough such that the two beams will not knock away or heat up the cold atoms. Such a short-pulse and slow-sweep method can minimize the deformation or asymmetry of spectra caused by the forces from the two beams. The pulse length is also made long enough such that measured spectra can be considered as steady-state results.

II. EXPERIMENTAL SETUP

We study the pump-probe spectroscopy in laser-cooled ^{87}Rb atoms. Our experimental arrangement is shown in Fig. 1. Cold ^{87}Rb atoms are produced with a vapor-cell MOT [18]. We maintain the pressure of Rb background vapor in the trapping cell at about 10^{-8} torr throughout the experiment. The MOT is formed with a spherical quadrupole magnetic field, six trapping laser beams, and a repumping laser beam. Two anti-Helmholtz coils generate the spherical quadrupole magnetic field with an axial gradient of 7.8 G/cm. The circular trapping beams have $1/e$ diameters of 9.6 mm and the power of each trapping beam is about 2.3 mW. Its frequency is tuned to 14 MHz below the $|F=2\rangle \rightarrow |F'=3\rangle$ transition. (F indicates a hyperfine level in the $5S_{1/2}$ ground state and F' indicates that in the $5P_{3/2}$ excited state. Such notations are used throughout this article.) The repumping beam drives the $|F=1\rangle \rightarrow |F'=2\rangle$ transition with an $1/e$ diameter of 10 mm and a power of 4 mW. The temperature of the cold atoms is about 250 μK measured with the delayed-image technique [19,20].

The pump beam is in elliptical shape with major and minor $1/e$ diameters of 3.9 mm and 2.9 mm. Cold atoms produced by the MOT are completely inside this $1/e$ beam profile of the pump field. The probe beam is sent through a circular aperture with a diameter of 0.8 mm, before it interacts with the atoms. Its intensity is rather uniform. We keep the power of the circular probe beam at $5\,\mu$W in the experiment. The pump and probe beams propagate in the orthogonal directions in most measurements. In this paper, the angle between the propagation directions is 90°, if we do not specify the propagation directions of the two beams. The pump and probe beams can be linearly or circularly polarized in the experiment. To produce linearly polarized pump and probe beams, we use such polarizers that have the extinction ratio better than 10^4. The circularly polarized pump beam is produced with a quarter-wave plate. We carefully adjust the quarter-wave plate such that the ratio of σ_+ light to σ_- light or vice versa is greater than 300. The polarizing optics are always the last items in the optical paths before the beams enter the trapping cell and interact with the atoms.

The pump and probe beams come from two diode lasers, both of which are injection locked by the same master laser. An external-cavity diode laser is the master laser. Its frequency is locked to the center of the crossover line between the $|F=2\rangle \rightarrow |F'=2\rangle$ and $|F=2\rangle \rightarrow |F'=3\rangle$ transitions of ^{87}Rb atoms in the saturated absorption spectroscopy. The spectral linewidth of the master laser is less than 1 MHz. One beam from the master laser is sent through an acousto-optic modulator (AOM) and the diffracted output beam from the AOM seeds the pump laser. We adjust the driving frequency of the AOM to change the pump frequency. Another beam from the master laser is sent through another AOM in the double-pass configuration [21]. The twice-diffracted output beam from this AOM seeds the probe laser. The driving frequency of the AOM is modulated during the spectrum measurement to sweep the probe frequency. This double-pass configuration ensures that the optical alignment of the injection locking of the probe laser remains unchanged when the probe frequency is swept. We typically sweep the probe frequency at a speed of about 14 MHz/s.

The timing sequence of the experiment is shown in Fig. 1(c). We turn off the trapping beams of the MOT periodically. This is achieved with a mechanical chopper having a

modified blade. A photodiode monitors the light of the trapping beams after the chopper and sends its output signal to a circuit that can generate delayed pulses. Each delayed pulse is triggered by the falling edge of the signal from the photodiode. We adjust the delay time of the pulse to ensure that the trapping beams are completely off when the pump and probe beams are being turned on. The pulse switches on the pump and probe beams via two AOM's. We keep the driving frequencies of these two AOM's constant in the entire experiment. After the probe beam interacts with the atoms, its power is measured by a photodiode. A lock-in amplifier detects the output of this photodiode and generates the spectra. The pulse that controls the switching of the probe beam is also the reference signal of the lock-in amplifier. We set the pulse width to 8 μs to prevent the cold atoms from being knocked away or heated up by the pump and probe beams. The repumping beam of the MOT is always unblocked. Its frequency is far away from the studied transition and we expect the presence of the repumping beam influences the measured spectra little. The magnetic field of the MOT is kept on all the time, since we are not able to switch it off fast enough. To minimize the influence of the magnetic field on the spectra, we use a smaller magnetic-field gradient of 7.8 G/cm in this experiment than the optimum one.

In the measurements of the spectra, the frequency of the pump is fixed and the probe frequency is swept over the pump frequency. We have adjusted the pump frequency to red detunings and blue detunings of the $|F=2\rangle \rightarrow |F'=3\rangle$ transition for the study. The absolute frequency is calibrated with the absorption spectrum of the $|F=2\rangle \rightarrow |F'=3\rangle$ transition of cold ^{87}Rb atoms. When measuring the probe spectrum for the calibration, we use the linearly polarized probe field and do not turn on the pump field. The axial magnetic-field gradient of the MOT is further reduced to 3.9 G/cm in the calibration. The timing sequence of switching the trapping and probe fields and the measurement method are the same as those described before. The measured spectra have the typical width of around 8 MHz and the run-to-run fluctuation of their peak positions is about 1 MHz. Having found the driving frequencies of the injection-locking AOM and the chopping AOM of the probe field with respect to the peak of the calibration spectrum, we deduce the absolute frequency of the master laser. Once the master laser frequency is calibrated, the pump and probe frequencies in the experimental data are obtained.

III. THEORETICAL CALCULATIONS

We have performed two theoretical calculations to identify the mechanisms behind the observed spectra and to examine the experimental data. In one calculation, we consider the transitions between the excited- and ground-state Zeeman levels. This is the Zeeman-state calculation. In our second calculation, we consider the transitions between momentum states of the atoms. It is called the momentum-state calculation. The Zeeman-state and momentum-state calculations will be described below.

A. The Zeeman-state calculation

We use density-matrix approach to calculate probe absorption spectra [22–24]. In the calculation, the z axis (quantization axis) is chosen according to the polarization of the strong pump field [24]. If the pump field is linearly polarized, the quantization axis is in the polarization direction of the pump field. If the pump field is circularly polarized, the quantization axis is in the propagation direction of the pump field. The total Hamiltonian of the system consists of four parts as shown in the following:

$$H_{\text{atom}} = \hbar\omega_0 \sum_{m_e=-3}^{3} |m_e\rangle\langle m_e|, \tag{1}$$

$$H_{\text{pump}} = \left(-\frac{\hbar\Omega}{2} e^{i\omega t} \sum{}' \, C_{m_e m_g} |m_g\rangle\langle m_e| \right) + \text{c.c.}, \tag{2}$$

$$H_{\text{probe}} = \left(-\frac{\hbar\Omega'}{2} e^{i\omega' t} \sum{}' \, C_{m_e m_g} |m_g\rangle\langle m_e| \right) + \text{c.c.}, \tag{3}$$

$$H_{\text{Zeeman}} = \mu_B B_0 \left(g_2 \sum_{m_g=-2}^{2} m_g |m_g\rangle\langle m_g| + g_3 \sum_{m_e=-3}^{3} m_e |m_e\rangle\langle m_e| \right). \tag{4}$$

In the above equations, $|m_g\rangle$ denotes the Zeeman sublevel of the $|F=2\rangle$ ground state and $|m_e\rangle$ denotes that of the $|F'=3\rangle$ excited state. Notation Σ' means summation over all allowed transitions that depend on the polarization of the laser field. H_{atom} is the atom Hamiltonian and ω_0 is the unperturbed $|F=2\rangle \rightarrow |F'=3\rangle$ transition frequency, H_{pump} and H_{probe} are the Hamiltonians of the pump and probe fields, ω is the pump frequency, Ω is the Rabi frequency defined as $\sqrt{I/2I_0}\Gamma$, where I is the pump field intensity, I_0 is the saturation intensity of the $|F=2, m_g=2\rangle \rightarrow |F'=3, m_e=3\rangle$ transition, and Γ is the spontaneous decay rate of the $5P_{3/2}$ excited state. ω' and Ω' indicate the similar physical quantities of the probe field. $C_{m_e m_g} \equiv \langle F'=3, m_e | F=2, m_g; 1, m_e - m_g \rangle$ is the Clebsch-Gordan coefficient. The equations of H_{pump} and H_{probe} are written under the rotating wave approximation. H_{Zeeman} is the Hamiltonian of the Zeeman shifts induced by a static magnetic field B_0 in the direction of the quantization axis. μ_B is the Bohr magneton, and g_2 and g_3 are the g factors of the $|F=2\rangle$ and $|F'=3\rangle$ states.

The steady state of the density matrix ρ of the system is solved with the equation below:

$$\frac{d\rho}{dt} = \frac{1}{i\hbar}[H_{\text{atom}} + H_{\text{pump}} + H_{\text{Zeeman}} + H_{\text{probe}}, \rho] + \left\{ \frac{d\rho}{dt} \right\}, \tag{5}$$

where $\{d\rho/dt\}$ describes the relaxation of ρ. The relaxation due to the spontaneous decay, collisions, and magnetic-field inhomogeneity is taken into account. Since the pump and probe lasers are injection locked by the same master laser,

we do not consider laser-linewidth effects in $\{d\rho/dt\}$ [25]. We write down all the matrix elements of $\{d\rho/dt\}$ in the following:

$$\left\{\frac{d\rho_{m_e m_e}}{dt}\right\} = -(\Gamma+\gamma_c)\rho_{m_e m_e}, \tag{6}$$

$$\left\{\frac{d\rho_{m_g m_g}}{dt}\right\} = \Gamma\left(\sum_{m_e=m_g-1}^{m_g+1} C^2_{m_e m_g}\rho_{m_e m_e}\right) + \gamma_c\left(\sum_{m_e=-3}^{3}\frac{\rho_{m_e m_e}}{5}\right) - \gamma_c\left(\rho_{m_g m_g} - \sum_{m'_g=-2}^{2}\frac{\rho_{m'_g m'_g}}{5}\right), \tag{7}$$

$$\left\{\frac{d\rho_{m_g m_e}}{dt}\right\} = -\left(\frac{\Gamma}{2}+\mu_B\gamma_b|g_2 m_g - g_3 m_e| + \gamma_c\right)\rho_{m_g m_e}, \tag{8}$$

$$\left\{\frac{d\rho_{m_e m'_e}}{dt}\right\} = -(\Gamma+\mu_B\gamma_b|g_3 m_e - g_3 m'_e| + \gamma_c)\rho_{m_e m'_e}, \tag{9}$$

$$\left\{\frac{d\rho_{m_g m'_g}}{dt}\right\} = \Gamma\left(\sum_{\Delta m=\Delta m'=0,\pm 1} C_{m_e m_g}C_{m'_e m'_g}\rho_{m_e m'_e}\right) - (\mu_B\gamma_b|g_2 m_g - g_2 m'_g| + \gamma_c)\rho_{m_g m'_g}, \tag{10}$$

where γ_c is the collision rate and γ_b describes the relaxation due to magnetic-field inhomogeneity in the direction of the quantization axis. Because the collision rate in the cold atoms is much smaller than other relaxation rates, we always put $\gamma_c = 0.001\Gamma$ in the calculation. In the last equation, $\Delta m = m_e - m_g$ and $\Delta m' = m'_e - m'_g$. Treating the weak H_{probe} as the perturbation, we carry out the calculation to all orders of $H_{\text{atom}} + H_{\text{pump}} + H_{\text{Zeeman}}$ and to the first order of H_{probe}. After the stationary solution of Eq. (5) is found numerically, the probe absorption cross section is the imaginary part of

$$\frac{3\lambda^2}{2\pi}e^{i\omega' t}\sum{}' \rho_{m_e m_g}C_{m_e m_g}\Gamma/\Omega'. \tag{11}$$

In the above formula, the notation of Σ' is the summation for all allowed probe transitions.

B. The momentum-state calculation

The spectra of the stimulated Raman transition between differently populated momentum states are calculated [26–29]. Such transition is also called the recoil-induced resonance (RIR). The transition process is that an atom absorbs a pump photon and once stimulated emits a probe photon, or vice versa. Depending on the population difference between the two momentum states linked by the pump and probe fields, the probe field can be amplified or absorbed. Considering that the pump and probe frequencies are far from the $|F=2\rangle \rightarrow |F'=3\rangle$ resonance and assuming that the y axis is parallel to the direction of the recoil momentum, the probe amplification is proportional to

$$\frac{1}{\sqrt{2\pi m k_B T}}\int_{-\infty}^{\infty} \times dp_y \frac{\gamma(\exp(-p_y^2/2mk_BT) - \exp(-p_y'^2/2mk_BT))}{\gamma^2 + 4\left[\frac{p_y'^2}{2m} - \left(\frac{p_y^2}{2m} + \hbar\omega - \hbar\omega'\right)\right]^2}. \tag{12}$$

In the above, m is the mass of the atoms, T is the temperature of the atoms, k_B is the Boltzmann constant, γ is the relaxation rate of the system, and p_y and p'_y are the initial and final momentums of the transition. According to the momentum conservation, p'_y relates to p_y as the following:

$$p'_y \approx p_y + \frac{2\hbar\omega_0}{c}\sin\frac{\theta}{2}, \tag{13}$$

where θ is the angle between the propagation directions of the pump and probe beams. We obtain theoretical RIR spectra by numerically evaluating the above integral.

From the results of the calculation, we notice that the RIR spectral profile is dispersive and centers around $\omega' = \omega$ [28]. The width of the profile increases both with T and with θ. The dependence on θ of the width is less significant at larger angles. If γ is negligible, the amplitude of the RIR profile is independent of θ. On the other hand, a non-negligible γ will reduce the amplitude and such reduction is more pronounced at smaller angles.

IV. EXPERIMENTAL DATA AND DISCUSSION

There are four polarization configurations of the pump and probe fields experimentally studied. (i) Both fields are linearly polarized in the same direction. This is the $lin\|lin$ configuration. (ii) Both fields are linearly polarized and their polarization directions are orthogonal. This is the $lin\perp lin$ configuration. (iii) The pump field is circularly polarized and the probe field is linearly polarized in the direction parallel to the propagation direction of the pump field. This is the $\sigma\|lin$ configurations. (iv) The pump field is circularly polarized and the probe field is linearly polarized in the direction normal to the propagation direction of the pump field. This is the $\sigma\perp lin$ configuration. Figure 2 shows typical spectra of these four configurations. The spectra in the left and the right columns of the figure are under red- and blue-detuned pump fields, respectively. For different polarization configurations, not only the spectral profiles exhibit variety but also the symmetries between the left and the right columns behave differently. We will present and discuss the data in Secs. IV A–IV E five sections. Sections IV A–IV D are for the four polarization configurations. Section IV E includes the discussion of the polarization configurations other than the above four. It also demonstrates the spectra containing two-wave mixing signals.

We summary the notations that will be used later. Δ is the detuning of the pump field from the $|F=2\rangle \rightarrow |F'=3\rangle$ resonance. Ω is the Rabi frequency of the pump field as defined previously. $\delta = \omega' - \omega$ is the difference between probe and pump frequencies. θ is the angle between pump and probe propagation directions.

All the spectral plots presented later will have the follow-

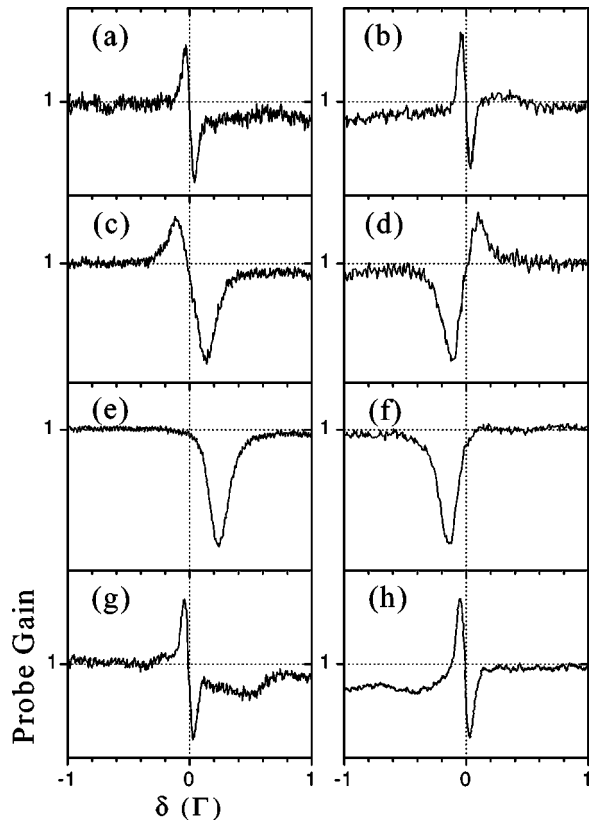

FIG. 2. Experimental pump-probe spectra in different polarization configurations. (a) and (b) are in $lin\|lin$. (c) and (d) are in $lin\perp lin$. (e) and (f) are in $\sigma\|lin$. (g) and (h) are in $\sigma\perp lin$. The horizontal scales of all the plots are the same. $\Delta=-4.2\Gamma$ for the spectra in the left column and $\Delta=4.1\Gamma$ for spectra in the right column. $\Omega=(4\pm0.9)\Gamma$ for all the spectra.

ing conventions. The horizontal scales are in the unit of the spontaneous decay rate. The natural linewidth of the $5P_{3/2}$ excited state is 5.9 MHz. In the vertical axes, values of probe gain larger than 1 indicate amplification of the probe field and those smaller than 1 indicate absorption of the probe field.

A. $lin\|lin$

The result from the Zeeman-state calculation in the $lin\|lin$ configuration shows a typical Mollow spectrum. Such results are expected, since the excitations of the pump and probe fields can be decomposed into several two-level systems as shown in Fig. 3(a). The dispersive profile around $\delta=0$ in the Mollow spectrum has a width much larger than that of the experimental data in Fig. 2(a). Its *polarity* is opposite to the *polarity* of the experimental data in Fig. 2(a). (We define the *polarity* of a dispersive profile as the following. The positive *polarity* means probe amplification for $\delta<0$ and probe absorption for $\delta>0$. The negative *polarity* means probe absorption for $\delta<0$ and probe amplification for $\delta>0$.) Clearly, the Zeeman-state calculation cannot predict the experimental observations in Figs. 2(a) and 2(b). There is other evidence to show that the experimental $lin\|lin$ spectra are not due to the transitions between Zeeman states. If we

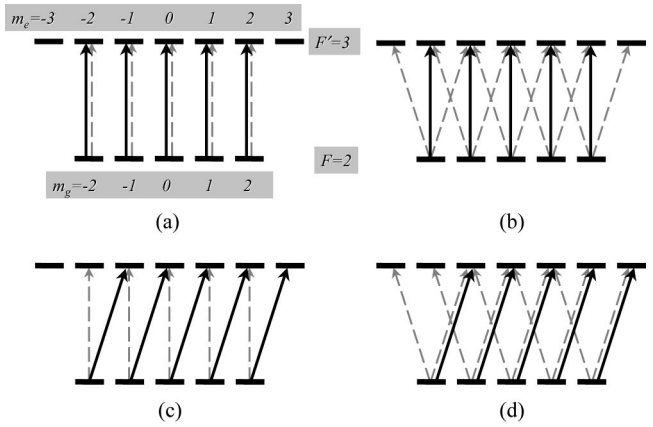

FIG. 3. The excitations of the pump and probe fields in different configurations. (a) $lin\|lin$, (b) $lin\perp lin$, (c) $\sigma\|lin$, and (d) $\sigma\perp lin$. Solid lines indicate pump excitations and dashed lines indicate probe excitations.

increase the magnetic-field gradient by a factor of 2, the observed spectra are broadened little. This implies that the Zeeman states play little roles in the $lin\|lin$ spectra.

The experimental spectra in the $lin\|lin$ configuration are the consequences of RIR. Figure 4 shows the spectra at four different θs. The widths of the spectra increase with θ. The amplitudes of the spectra are nearly the same at $\theta=50°, 90°$, and 125°. Only the amplitude of the spectrum at $\theta=15°$ gets much smaller. The *polarities* of the dispersive

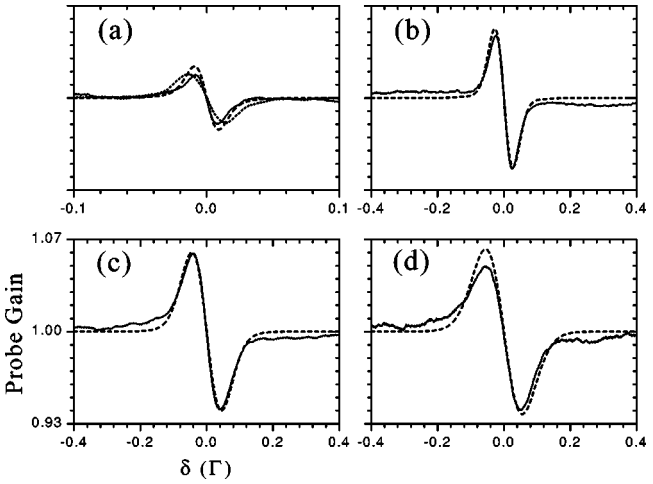

FIG. 4. The pump-probe spectra in the $lin\|lin$ configuration. Solid lines are experimental data and dashed lines are theoretical curves from the momentum-state calculation. The dotted line in (a) is also an experimental spectrum. $\Delta=-7\Gamma$ and $\Omega=(6.7\pm1.5)\Gamma$. $\theta=15°$ in (a), 50° in (b), 90° in (c), and 125° in (d). All the theoretical curves correspond to $T=200$ μK and $\gamma=2\pi\times80$ kHz. The vertical scales of all the plots are the same. We measure the spectrum of the solid line in (a) with a pulse width of 16 μs, instead of 8 μs used elsewhere in this paper. The spectrum of the dotted line in (a) is measured with a pulse width of 8 μs and clearly shows the transit-time broadening. Using a pulse width of 16 μs does not change the spectra in (b), (c), and (d). Using $\gamma=0$ in the calculation modifies the spectra in (b), (c), and (d) little.

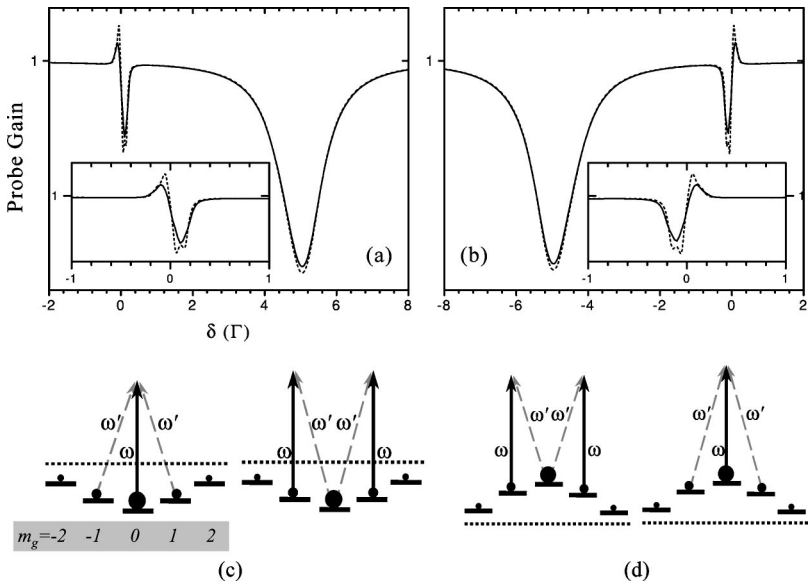

FIG. 5. The $lin\perp lin$ configuration: (a) and (b) are the spectra from the Zeeman-state calculation. The insets of (a) and (b) display the spectra in the range of $-\Gamma<\delta<\Gamma$ and their vertical scales are magnified by two folds. $\Omega=4\Gamma$ for all the spectra and $\Delta=-4.2\Gamma$ in (a) and 4.1Γ in (b). Solid lines are calculated with $B_0=-0.3$ G and $\gamma_b=0.1$ G. Dashed lines are calculated with $B_0=0$ and $\gamma_b=0$. (c) and (d) are the light shifts and the population distribution of ground-state Zeeman sublevels. The size of the solid circle indicates the population distribution and the dotted horizontal line indicates the unperturbed energy level. (c) $\Delta<0$ and (d) $\Delta>0$. We only draw Raman transitions among $|m=0,\pm1\rangle$ states for simplicity and the contributions from other Raman transitions are similar.

profiles are independent of the sign of Δ and are always positive. All the experimental observations are consistent with the predictions of the momentum-state calculation as described in Sec. III B. We fit the experimental data with the theoretical curves from the momentum-state calculation. The best fits of the four θs consistently indicate a temperature of 200 μK and a relaxation rate γ of $2\pi\times80$ kHz as shown in Fig. 4. This temperature is close to the temperature measured by the delayed-image method.

References [30,31] provide detailed information for measuring temperatures with RIR spectra. According to the studies of these references, we feel that the method of short pulse and slow sweep is very suitable for measuring temperatures with RIR spectra. The short pulse can prevent the heat up of cold atoms from the pump and probe fields. It can also allow the pump and probe fields with higher intensities in order to produce larger RIR signals. The slow scan with the lock-in detection can greatly enhance signal-to-noise ratio. Furthermore, RIR spectra with larger θs have the advantage that the spectral width is less sensitive to the θ, the relaxation rate of the system, and the transit effect. RIR spectra in small θs have smaller linewidths and are more sensitive to the relaxation rate of the system. They also require longer interaction time to reach steady states [31] and are more easily influenced by the transit-time broadening. Such broadening is demonstrated in Fig. 4(a). We have compared the temperature sensitivities of the RIR spectra in $\theta=90°$ and in $\theta=10°$ by using the momentum-state calculation with $\gamma\rightarrow0$. At 30 or 300 μK, a 10% decrease in temperature results in about 5% change in spectral width of $\theta=90°$ and results in about the same amount of change in the spectral width of $\theta=10°$. The temperature sensitivities of the two θs are comparable. This suggests that RIR spectra with larger θs are better for the temperature measurement because they are more immune from the uncertainties of the experimental conditions.

B. $lin\perp lin$

The spectral profiles in this polarization configuration are dispersionlike, but are clearly different from the RIR spectral profiles. As shown in the spectra of Figs. 2(c) and 2(d), the amplitude of amplification is less than that of absorption; the *polarities* of the positive and negative Δ's are opposite. The Zeeman-state calculation in the $lin\perp lin$ configuration predicts the spectra in agreement with the above experimental observations. The spectra from the calculation are shown in Figs. 5(a) and 5(b).

The dispersionlike shapes and the *polarities* can be explained by the theory of the stimulated Raman transitions between ground-state Zeeman levels in Ref. [13]. Figure 3(b) shows the excitations of the pump and probe fields. The pump field drives $\Delta m=0$ transitions and the probe field drives $\Delta m=\pm1$ transitions. For a negative Δ, the light shifts of ground-state Zeeman levels induced by the pump field and the population distribution determined by the optical pumping due to the pump field, are shown in Fig. 5(c). With the two-photon transitions drawn in Fig. 5(c), amplification of the probe field occurs when $\delta<0$ and absorption of the probe field occurs when $\delta>0$. The *polarity* of the dispersionlike profile is positive. For a positive Δ, the light shifts of ground-state Zeeman levels induced by the pump field and the population distribution determined by the optical pumping due to the pump field, are depicted in Fig. 5(d). Absorption of the probe field occurs when $\delta<0$ and amplification of the probe field occurs when $\delta>0$. The *polarity* of the dispersionlike profile is negative.

In the insets of Figs. 5(a) and 5(b), the spectra of the dashed lines show two absorption peaks. This is because the stimulated Raman transitions can happen, not only between $|m=0\rangle$ and $|m=\pm1\rangle$, but also between $|m=\pm1\rangle$ and $|m=\pm2\rangle$. The resonance condition of the transition between $|m=0\rangle$ and $|m=\pm1\rangle$ differs from that of the transition between $|m=\pm1\rangle$ and $|m=\pm2\rangle$. There are also two amplification peaks in the spectra, but they cannot be clearly seen. The two absorption peaks and the two amplification peaks can be resolved better, when the light shifts of the Zeeman levels become larger by increasing the Rabi frequency of the pump field. Our experimental data do not demonstrate such spectra of two absorption peaks and two amplification peaks,

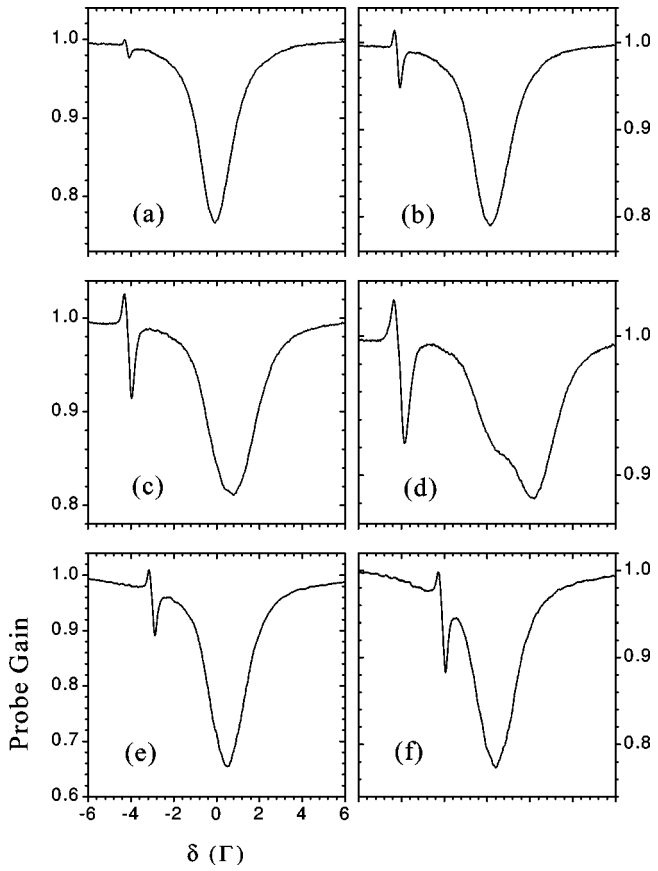

FIG. 6. The experimental $lin\perp lin$ spectra at several Ω's and Δ's. The horizontal scales of all the plots are the same. (a) $\Omega=(2.1\pm0.5)\Gamma$ and $\Delta=-4.2\Gamma$. (b) $\Omega=(3.3\pm0.8)\Gamma$ and $\Delta=-4.2\Gamma$. (c) $\Omega=(4.5\pm1)\Gamma$ and $\Delta=-4.2\Gamma$. (d) $\Omega=(6.5\pm1.5)\Gamma$ and $\Delta=-4.2\Gamma$. (e) $\Omega=(3.1\pm0.7)\Gamma$ and $\Delta=-3.1\Gamma$. (f) $\Omega=(3.1\pm0.7)\Gamma$ and $\Delta=-2.0\Gamma$.

since the magnetic field of the MOT is not turned off during the measurements and it broadens the peaks.

The unequal amplitudes of amplification and absorption in the spectra can also be explained by the stimulated Raman transitions. In the absorption cases, the product of the squares of the two Clebsch-Gordan coefficients involved in the two-photon transitions is 16/75. In the amplification cases, the product of the squares of the two Clebsch-Gordan coefficients involved in the two-photon transitions is 3/25. Comparing these two numbers, we immediately know that the two-photon transition rate of the probe absorption is larger than that of the probe amplification. The ratio of these two numbers is close to the ratio of the absorption amplitude to the amplification amplitude in the experimental spectra of Figs. 2(c) and 2(d).

We plot the experimental $lin\perp lin$ spectra at several Ω's and Δ's in Fig. 6. The spectra are taken in different dates and the number of atoms in each plot may not be same. The spectral amplitude increases with Ω and decreases with Δ. The spectral width behaves similarly. In general, the agreement between the experimental data and the theoretical predictions from the Zeeman-state calculation is satisfactory.

C. $\sigma\|lin$

The spectra in this polarization configuration exhibit Lorentzian profiles. As shown in Figs. 2(e) and 2(f), the frequency of the peak of the Lorentzian profile is larger than the pump frequency for a negative Δ and smaller than the pump frequency for a positive Δ. The Zeeman-state calculation in the $\sigma\|lin$ configuration predicts the spectra in agreement with the above experimental observations. The spectra from the calculation are shown in Figs. 7(a) and 7(b).

Following the idea of stimulated Raman transitions in Ref. [13], we can also explain the observed $\sigma\|lin$ spectra.

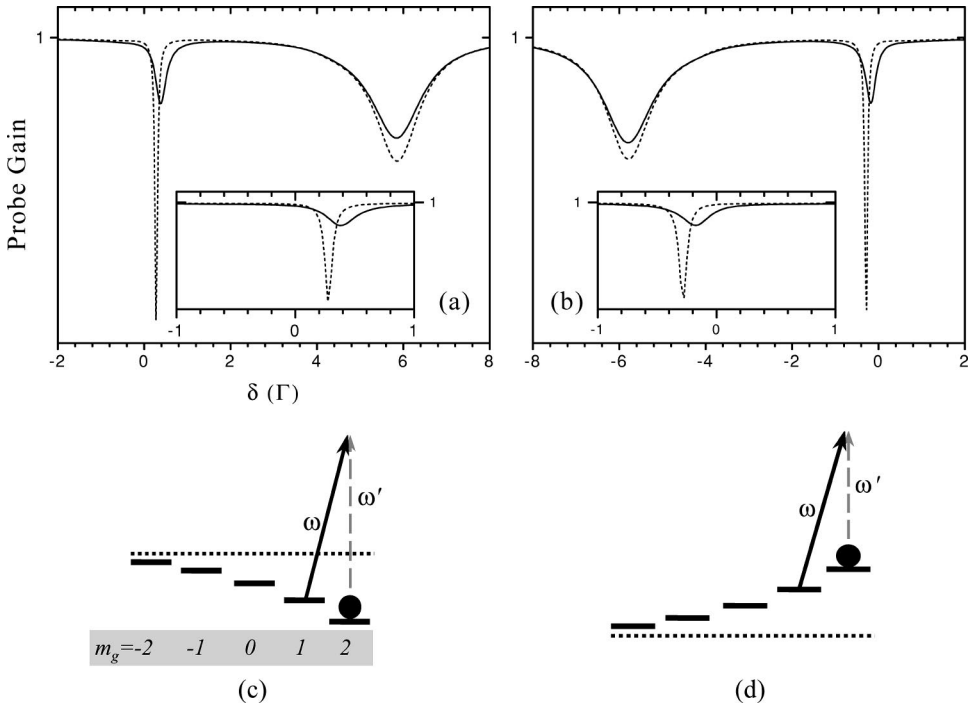

FIG. 7. The $\sigma\|lin$ configuration: (a) and (b) are the spectra from the Zeeman-state calculation. The insets of (a) and (b) display the spectra in the range of $-\Gamma<\delta<\Gamma$. $\Omega=4\Gamma$ for all the spectra and $\Delta=-4.2\Gamma$ in (a) and 4.1Γ in (b). Solid lines are calculated with $B_0=-0.8$ G and $\gamma_b=0.8$ G. Dashed lines are calculated with $B_0=0$ and $\gamma_b=0$. (c) and (d) are the light shifts and the population distribution of ground-state Zeeman sublevels. The solid circle indicates the population and the dotted-horizontal line indicates the unperturbed energy level. (c) $\Delta<0$ and (d) $\Delta>0$.

For all the presented $\sigma \| lin$ spectra, the pump field is in the σ_+ polarization. We just discuss the σ_+ pump field and the outcomes of the σ_- pump field are similar. Figure 3(c) depicts the excitations of the pump and probe fields. Since the σ_+ pump field can put nearly all population to the $|m_g=2\rangle$ state, only the transitions involving the $|m_g=2\rangle$ state need to be concerned. The light shifts and the population distribution of the ground-state Zeeman levels caused by the pump field are illustrated in Figs. 7(c) and 7(d). The two-photon transitions from $|m_g=2\rangle$ to $|m_g=1\rangle$ drawn in the figure result in the observed spectra of probe absorption. It is clear in the figure that the probe frequency of the two-photon resonance is larger than the pump frequency for $\Delta<0$ and smaller than the pump frequency for $\Delta>0$. The situation shown in the figure also indicates that amplification of the probe field cannot occur.

The peak position of the experimental spectrum in Fig. 2(f) is closer to $\delta=0$ than that in Fig. 2(e). It indicates that a magnetic field is present in the experimental system and its direction is opposite to the propagation direction of the σ_+ pump field. Since the quantization axis is pointing to the propagation direction of the pump field, this magnetic field is negative. The negative magnetic field shifts $|m_g=2\rangle$ away from $|m_g=1\rangle$ in Fig. 7(c) and shifts $|m_g=2\rangle$ toward $|m_g=1\rangle$ in Fig. 7(d). Consequently, the peak position of the spectrum moves toward $\delta=0$ for a positive Δ and moves away from $\delta=0$ for a negative Δ. The solid lines in Figs. 7(a) and 7(b) are calculated with a negative B_0 and demonstrate such behaviors in the insets of the figures. The presence of the negative magnetic field is indeed expected in the experimental system, since the intensities of the counterpropagating trapping beams of our MOT are not equal and the cold atoms center around a position where the magnetic field is negative.

We plot the experimental and theoretical $\sigma \| lin$ spectra at $\Delta=-4.2\Gamma$ and several Ω's in Fig. 8. All the spectra are taken in one run. By increasing Ω, the spectral width gets broader and the peak position moves further away from the pump frequency. Both behaviors can be clearly seen in the experimental and theoretical curves. Furthermore, the experimental data are in agreement with the theoretical spectra. When fitting the experimental spectra, we find that the $|B_0|$ and γ_b, in the calculation of the best fit, increase with Ω. It can be interpreted that the pump field with a higher intensity pushes the cold atoms further away from the MOT center and spreads them further out. Since the pump field is in the σ_+ polarization and its propagation direction is almost the same as the propagation direction of the trapping beam with the higher intensity, the interpretation is reasonable.

In Fig. 8, each of the top two plots shows a small bump emerges at the left of the large Lorentzian profile. Because the peak of the bump appears at $\delta<0$, the bump cannot be explained by Raman transitions between the ground-state Zeeman levels drawn in Fig. 7(c) such as the transition from $|m_g=1\rangle$ to $|m_g=0\rangle$. The three-photon transition from $|m_e=3\rangle$ to $|m_g=1\rangle$ causes this bump. In the transition, two pump photons are emitted and one probe photon is absorbed. Since the resonance frequency between $|m_e=3\rangle$ and $|m_g=1\rangle$ is larger than the pump frequency, the probe frequency

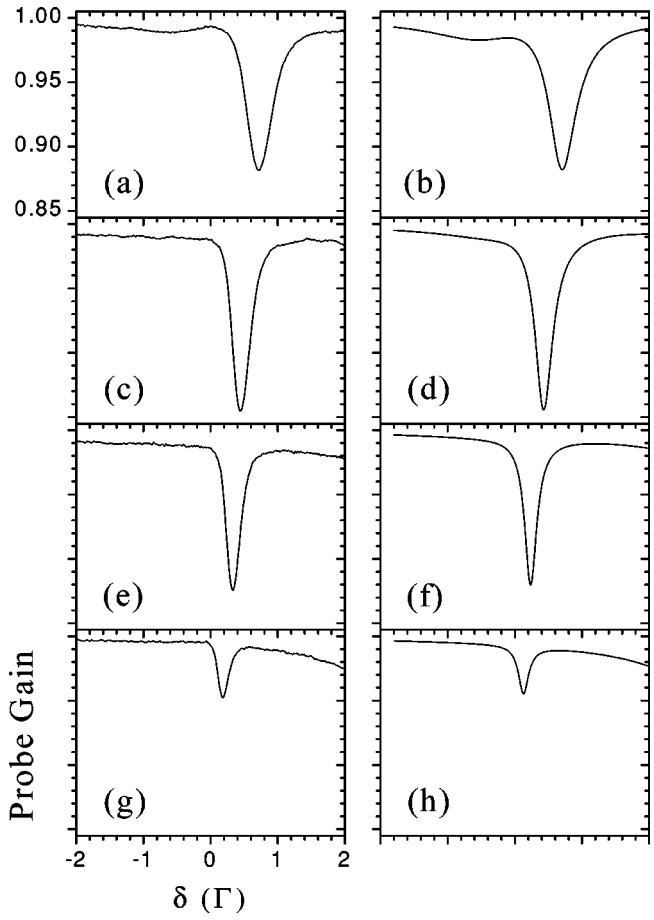

FIG. 8. The $\sigma \| lin$ spectra at $\Delta=-4.2\Gamma$ and several Ω's. The spectra in the left column are the experimental data and those in the right column are the theoretical curves from the Zeeman-state calculation. The vertical scales and the horizontal scales of all the plots are the same. (a) $\Omega=(6.5\pm1.5)\Gamma$. (b) $\Omega=7.5\Gamma$, $B_0=-1.0$ G, and $\gamma_b=1.0$ G. (c) $\Omega=(4.5\pm1)\Gamma$. (d) $\Omega=5.0\Gamma$, $B_0=-0.8$ G, and $\gamma_b=0.8$ G. (e) $\Omega=(3.3\pm0.8)\Gamma$. (f) $\Omega=3.0\Gamma$, $B_0=-0.7$ G, and $\gamma_b=0.7$ G. (g) $\Omega=(2.1\pm0.5)\Gamma$. (h) $\Omega=1.5\Gamma$, $B_0=-0.7$ G, and $\gamma_b=0.7$ G.

with respect to the three-photon resonance should be less than the pump frequency and the peak of the bump appears at $\delta<0$. The $|m_e=3\rangle$ state is far less populated than the $|m_g=2\rangle$ state. It can be understood that the amplitude of the bump is much smaller than that of the two-photon Raman transition from $|m_g=2\rangle$ to $|m_g=1\rangle$.

D. $\sigma \perp lin$

The experimental spectra in the $\sigma \perp lin$ configuration have two distinct structures: a dispersive profile and a small Lorentzian profile as shown in Figs. 2(g) and 2(h). The *polarity* of the dispersive profile is always positive for either a negative or a positive Δ. The frequency of the peak of the Lorentzian profile is larger than the pump frequency for a negative Δ and smaller than the pump frequency for a positive Δ. We will explain in the next two paragraphs that the Lorentzian profile is due to the stimulated Raman transition between the ground-state Zeeman sublevels and the dispersive profile is due to the RIR.

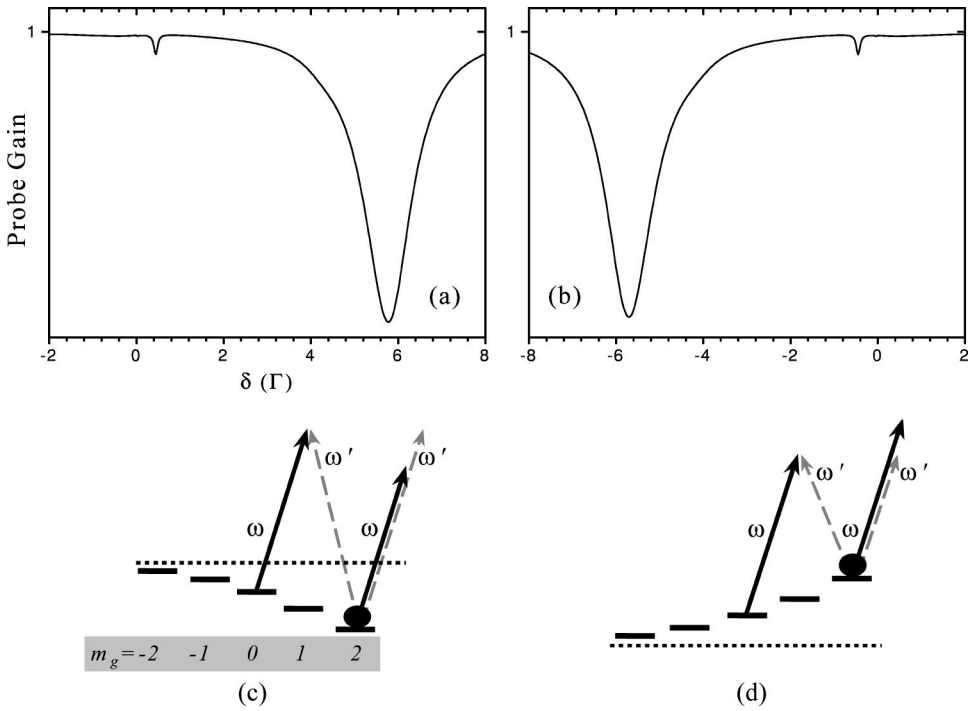

FIG. 9. The $\sigma\perp lin$ configuration: (a) and (b) are the spectra from the Zeeman-state calculation. $\Delta=-4.2\Gamma$ in (a) and 4.1Γ in (b). The both spectra are calculated with $\Omega=4\Gamma$, $B_0=0$, and $\gamma_b=0$. (c) and (d) are the light shifts and the population distribution of ground-state Zeeman sublevels. The solid circle indicates the population and the dotted-horizontal line indicates the unperturbed energy level. (c) $\Delta<0$ and (d) $\Delta>0$.

For the excitations of the pump and probe fields as shown in Fig. 3(d), the light shifts and the population distribution of the ground-state Zeeman levels caused by the pump field are illustrated in Figs. 9(c) and 9(d). Almost all population is in the $|m_g=2\rangle$ state, because of the optical pumping by the circularly polarized pump field. In Figs. 9(c) and 9(d), the two-photon transition from $|m_g=2\rangle$ to $|m_g=0\rangle$ results in the Lorentzian profile of the probe absorption. The Zeeman calculation predicts such profiles in Figs. 9(a) and 9(b) and the positions of the peaks of the profiles are consistent with the experimental observations. We point out that the product of the squares of the two Clebsch-Gordan coefficients, involved in the two-photon transition from $|m_g=2\rangle$ to $|m_g=0\rangle$, is 2/75. On the other hand, the product of the squares of the two Clebsch-Gordan coefficients, involved in the two-photon transition from $|m_g=2\rangle$ to $|m_g=1\rangle$ of the $\sigma\|lin$ configuration, is 2/9. It comes as no surprise that the amplitude of the Lorentzian profile in the $\sigma\perp lin$ configuration is much smaller than that in the $\sigma\|lin$ configuration.

Figures 9(c) and 9(d) show that the pump and probe fields both drive the $|m_g=2\rangle$ to $|m_e=3\rangle$ transition. With the same discussion described in the subsection of $lin\|lin$, such excitations result in RIR spectra. The experimental observations also support the argument.

The pump field of Fig. 2(g) is in the σ_+ polarization and that of Fig. 2(h) is in the σ_- polarization. When we use the σ_+ pump field to measure the spectrum of $\Delta=4.1\Gamma$, the Raman-transition profile overlaps the RIR profile and the two profiles are not as distinguishable as the ones in Fig. 2(h). This is again due to the presence of the magnetic field in the experimental system whose direction is opposite to the propagation direction of the pump field. The RIR profile centered at $\delta=0$ is not affected by the magnetic field, but the Raman-transition profile is shifted toward $\delta=0$ by this magnetic field under the σ_+ pump field of $\Delta=4.1P$. Therefore, we use the σ_- pump field in the measurement of Fig. 2(h) to avoid the overlap of the two profiles.

We now discuss the unclear results in Ref. [13]. In that experiment, the propagation directions of the pump and probe fields are nearly collinear with an angle of about 20 mrad. The dispersionlike profiles are observed only when the pump field is circularly polarized. The peak-to-peak separation of the profile is about 2 MHz. The *polarity* of the dispersionlike profile is positive for a negative Δ and is negative for a positive Δ. Since the authors of Ref. [13] claim that they do not observe any polarization dependence of the probe field, we consider that the probe field is linearly polarized. In that case, their pump-probe polarization configuration is the same as the $\sigma\perp lin$ configuration. Our paper shows the Raman transitions in the $\sigma\perp lin$ configuration result in a Lorentzian profile of probe absorption, so the above experimental observations should not be explained by Raman transitions between ground-state Zeeman levels as they described. (Even if the pump and probe fields are both circularly polarized, the Raman transitions still result in a Lorentzian profile of probe absorption. This case will be discussed in the next section.) The above dispersionlike profiles are not due to the RIR, either. This is because the observed *polarities* are inconsistent with the *polarities* of the RIR spectra. Those experimental results in Ref. [13] have not been resolved.

E. Others

In the polarization configuration that the pump and probe are both circularly polarized and are in the same helicity, we can expect the RIR spectra. In the polarization configuration that the pump and probe are both circularly polarized and are in the opposite helicities, we can expect the Lorentzian profiles. The Lorentzian profiles are due to the stimulated Raman transition between the ground-state Zeeman sublevels. The above two configurations are just the two components of the $\sigma\perp lin$ configuration.

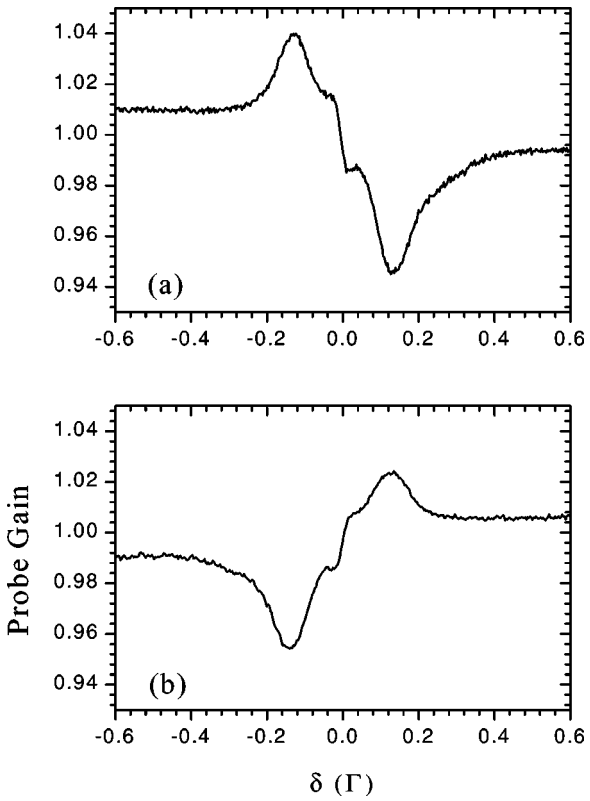

FIG. 10. The experimental pump-probe spectra in the $lin\perp lin$ configuration at $\theta=15°$. $\Omega=(4\pm0.9)\Gamma$. $\Delta=-4.2\Gamma$ in (a) and 4.1Γ in (b).

In the polarization configurations that the pump is linearly polarized and the probe is circularly polarized, we can expect the dispersionlike profiles. The dispersionlike profiles are due to the stimulated Raman transition between the ground-state Zeeman sublevels. Spectra of these two configurations should behave similar to those of the $lin\perp lin$ configuration.

When the pump and probe fields propagate in the directions with a small θ, the two-wave mixing signal will appear. Figure 10 shows the experimental $lin\perp lin$ spectra at $\theta=15°$. The very narrow structure inside the Raman profile and the very long tails outside the Raman profile are from the two-wave mixing. Its shape is similar to the two-wave mixing plot in Ref. [15]. The two-wave mixing signal gets smaller and then disappears with increasing θ. The *polarity* of the signal is positive for $\Delta<0$ and negative for $\Delta>0$. This is consistent with the prediction of the two-wave mixing theory for $J=3/2$ states in Ref. [15].

V. CONCLUSION

We have systematically studied the pump-probe spectra of cold ^{87}Rb atoms in various polarization configurations. The spectrum in the $lin\|lin$ configuration displays a dispersive profile and is due to the RIR. When the pump field is far off the resonance, the spectrum in the $lin\perp lin$ configuration shows a dispersionlike profile and the spectrum in the $\sigma\|lin$ configuration shows a Lorentzian profile. Both are caused by the stimulated Raman transitions between the ground-state Zeeman sublevels. The spectrum in the $\sigma\perp lin$ configuration displays a dispersive profile and a Lorentzian profile at a large detuning of the pump field. The dispersive profile results from the RIR and the Lorentzian profile is caused by the stimulated Raman transitions. Knowing the above results, we can derive all spectra in the other polarization configurations. Our paper provides essential information for the pump-probe spectroscopy of cold atoms.

ACKNOWLEDGMENTS

This work was supported by the National Science Council under NSC Grant No. 89-2112-M-007-048.

[1] E.L. Raab, M. Prentiss, A. Cable, S. Chu, and D.E. Pritchard, Phys. Rev. Lett. **59**, 2631 (1987).
[2] D. Grison, B. Lounis, C. Salomon, J.Y. Courtois, and G. Grynberg, Europhys. Lett. **15**, 149 (1991).
[3] J.W.R. Tabosa, G. Chen, Z. Hu, R.B. Lee, and H.J. Kimble, Phys. Rev. Lett. **66**, 3245 (1991).
[4] P. Verkerk, B. Lounis, C. Salomon, C. Cohen-Tannoudji, J.-Y. Courtois, and G. Grynberg, Phys. Rev. Lett. **68**, 3861 (1992).
[5] B. Lounis, J.-Y. Courtois, P. Verkerk, C. Salomon, and G. Grynberg, Phys. Rev. Lett. **69**, 3029 (1992).
[6] P.S. Jessen, C. Grez, P.D. Lett, W.D. Phillips, S.L. Rolston, R.J.C. Spreeuw, and C.I. Westbrook, Phys. Rev. Lett. **69**, 49 (1992).
[7] R.W. Fox, S.L. Gilbert, L. Hollberg, and J.H. Marquardt, Opt. Lett. **18**, 1456 (1993).
[8] N. Ph.Georigades, E.S. Polzik, and H.J. Kimble, Opt. Lett. **19**, 1474 (1994).
[9] A.G. Sinclair, B.D. McDonald, E. Riis, and G. Duxbury, Opt. Commun. **106**, 207 (1994).
[10] M.J. Snadden, A.S. Bell, E. Riis, and A.I. Ferguson, Opt. Commun. **125**, 70 (1996).
[11] M.J. Snadden, A.S. Bell, R.B.M. Clarke, E. Riis, and P.H. McIntyre, J. Opt. Soc. Am. B **14**, 544 (1997).
[12] J.L. Sørensen, J. Hald, and E.S. Polzik, Opt. Lett. **23**, 25 (1998).
[13] M. Mitsunaga, T. Mukai, K. Watanabe, and T. Mukai, J. Opt. Soc. Am. B **13**, 2696 (1996).
[14] G. Grynberg, M. Vallet, and M. Pinard, Phys. Rev. Lett. **65**, 701 (1990).
[15] M. Vallet, M. Pinard, and G. Grynberg, Opt. Commun. **87**, 340 (1992).
[16] J.-Y. Courtois and G. Grynberg, Phys. Rev. A **46**, 7060 (1992).
[17] J. Guo, Phys. Rev. A **49**, 3934 (1994).
[18] C. Monroe, W. Swann, H. Robinson, and C. Wieman, Phys. Rev. Lett. **65**, 1571 (1990).
[19] S. Kunze, G. Rempe, in *Laser Spectroscopy, XII International Conference*, edited by M. Inguscio, M. Allegrini, and A. Sasso (World Scientific, Singapore, 1996), p. 138.

[20] A. di Stefano, D. Wilkowski, J.H. Müller, and E. Arimondo, Appl. Phys. B **69**, 263 (1999).
[21] J. Ye, S. Swartz, P. Jungner, and J.L. Hall, Opt. Lett. **21**, 1280 (1996).
[22] A. Lezama, S. Barreiro, and A.M. Akulshin, Phys. Rev. A **59**, 4732 (1999).
[23] C. Cohen-Tannoudji, in *Frontier of Laser Spectroscopy*, edited by R. Balian, S. Haroche, and S. Liberman (North-Holland, Amsterdam, 1977), Vol. 1, pp. 28–73.
[24] Y.C. Chen, C.W. Lin, and I.A. Yu, Phys. Rev. A **61**, 053805 (2000).
[25] B.J. Dalton and P.L. Knight, J. Phys. B **15**, 3997 (1982).
[26] J. Guo, P.R. Berman, B. Dubetsky, and G. Grynberg, Phys. Rev. A **46**, 1426 (1992).
[27] J. Guo and P.R. Berman, Phys. Rev. A **47**, 4128 (1993).
[28] J.-Y. Courtois, G. Grynberg, B. Lounis, and P. Verkerk, Phys. Rev. Lett. **72**, 3017 (1994).
[29] P.R. Berman, B. Dubetsky, and J. Guo, Phys. Rev. A **51**, 3947 (1995).
[30] D.R. Meacher, D. Boiron, H. Metcalf, C. Salomon, and G. Grynberg, Phys. Rev. A **50**, R1992 (1994).
[31] S. Guibal, C. Triché, L. Guidoni, P. Verkerk, and G. Grynberg, Opt. Commun. **131**, 61 (1996).